Cell Reports
Physical Science

Article

EPR-refined atomistic molecular dynamics delivers predictive spectroscopy in self-organized soft matter systems

Graphical abstract

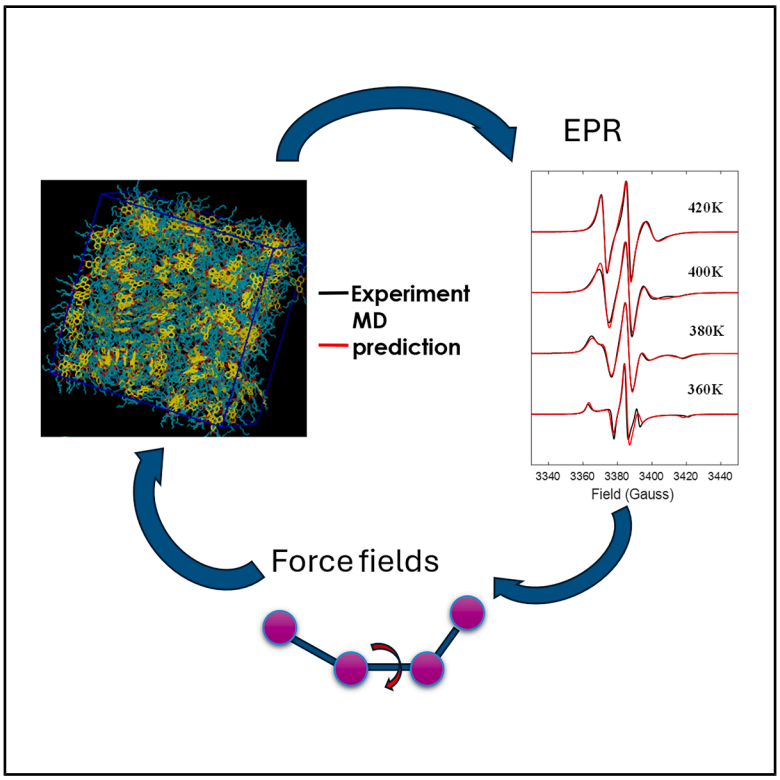

Authors

Mark Richard Wilson,
Vasily S. Oganesyan

Correspondence

mark.wilson@durham.ac.uk (M.R.W.),
v.oganesyan@uea.ac.uk (V.S.O.)

In brief

Wilson and Oganesyan report the use of EPR spectroscopy to evaluate and refine atomistic force fields for the discotic liquid crystal HAT6. Comparing experimental and MD-predicted spectra identifies improved parameters and reveals pretransitional stacking and emerging columnar order, all of which establishes EPR as a powerful benchmark for soft matter simulations.

Highlights

- EPR spectroscopy benchmarks and refines MD force fields for a discotic liquid crystal
- Subtle force field changes markedly alter predicted EPR line shapes
- Refined parameters reproduce EPR spectra and the isotropic-columnar transition temperature
- Atomistic MD reveals pretransitional columnar stacking and emergence of columnar order

Wilson & Oganesyan, 2026, Cell Reports Physical Science 7, 103332
June 17, 2026
https://doi.org/10.1016/j.xcrp.2026.103332

CellPress

Cell Reports
Physical Science

CellPress
OPEN ACCESS

Article

EPR-refined atomistic molecular dynamics delivers predictive spectroscopy in self-organized soft matter systems

Mark Richard Wilson[1,3,*] and Vasily S. Oganesyan[2,*]
[1]Department of Chemistry, Durham University, Science Laboratories, Stockton Road, Lower Mountjoy, Durham DH1 3QE, UK
[2]School of Chemistry, Pharmacy and Pharmacology, University of East Anglia, Norwich NR4 7TJ, UK
[3]Lead contact
*Correspondence: mark.wilson@durham.ac.uk (M.R.W.), v.oganesyan@uea.ac.uk (V.S.O.)
https://doi.org/10.1016/j.xcrp.2026.103332

SUMMARY

Electron paramagnetic resonance (EPR) spectroscopy with nitroxide spin probes is a sensitive probe of structural dynamics in soft matter. Here, we report the use of EPR to test and refine atomistic molecular dynamics (MD) force fields for the discotic liquid crystal 2,3,6,7,10,11 hexa(hexyloxy)triphenylene (HAT6). We show that subtle variations in partial charge schemes, aromatic core Lennard-Jones interactions, and alkoxy torsional potentials cause pronounced changes in predicted EPR line shapes. By comparing experimental and MD-predicted spectra at a reference temperature, we identify refined parameters that reproduce both the measured spectra and the isotropic-columnar phase transition temperature. The predictions reveal pre-transitional growth of short molecular stacks in the isotropic phase and the emergence of columnar order on cooling. This work establishes EPR spectroscopy as a powerful benchmark for testing and improving molecular force fields to deliver fully atomistic predictions of variable temperature EPR spectra of a discotic liquid crystal.

INTRODUCTION

Discotic liquid crystal (DLC) phases are formed from disc-shaped molecules, typically composed of planar or bowl-shaped aromatic cores, which are decorated with pendant aliphatic chains.[1] The disc-like molecular shape strongly promotes the stacking of molecules into columns, forming columnar liquid crystals with efficient charge transport, making them ideal candidates for organic electronics and photovoltaic devices. In most columnar phases, chains play a key role in stabilizing the columnar order through nanosegregation and providing flexibility that stabilizes liquid crystal ordering over crystallization. The one-dimensional ordering in these materials has led to promising research avenues for columnar phases as self-organized organic transport materials.[2–4]

Experimental probing of molecular structure in columnar-type materials is possible using X-ray and neutron scattering methods. These provide information on the nature of the second lattice type, intercolumnar distances, core-side chain segregation, and correlation length. To a lesser extent, information on dynamics is available through techniques, such as quasi-elastic neutron scattering (QENS) and inelastic neutron scattering (INS),[5–7] and through electron paramagnetic resonance (EPR) spectroscopy, taking advantage of careful doping of a columnar phase structure by an electron paramagnetic resonance EPR spin probe.[8]

Molecular simulation has played a vital role in helping to understand the structure of columnar phases.[3,9,10] Early atomistic simulations of pre-assembled hexabenzocoronene,[4] triphenylene,[9–11] and phthalocyanine-based[12] columnar phases demonstrated a substantial overlap of molecular cores, associated with π-stacking interactions, facilitating charge transport but with the presence of dynamical structural defects. Molecular modeling carried out in close combination with magnetic resonance spectroscopy can provide considerable enhancement to the information obtained from experiments.[13] Recent studies have shown that this approach provides unique insights into the structure of partially ordered soft matter systems such as lipid membranes,[14] smectic phases,[15] and molecular crystal solvates.[16] In contrast to traditional model-based interpretation approaches, which can sometimes lead to misleading kinetic data, the direct prediction of magnetic resonance spectra and relaxation times provides a faithful interpretation of complex multi-component motion.[16]

Crucial to all simulation studies is the molecular force field. Typical approaches to force field parametrization include the use of small-molecule studies to tune nonbonded parameters in combination with a suitable model for partial charges[17] and quantum chemical calculations to obtain information on bond stretching, bond bending, and torsional interactions (that are responsible for molecular flexibility). Machine learning can also be used to tune force fields if sufficiently reliable training data can be used.[18] Careful fitting of force fields for molecular fragments to reproduce densities is crucial to improving transition temperature predictions, because they tend to be highly sensitive to small errors in the predicted density.[17,19] We note,

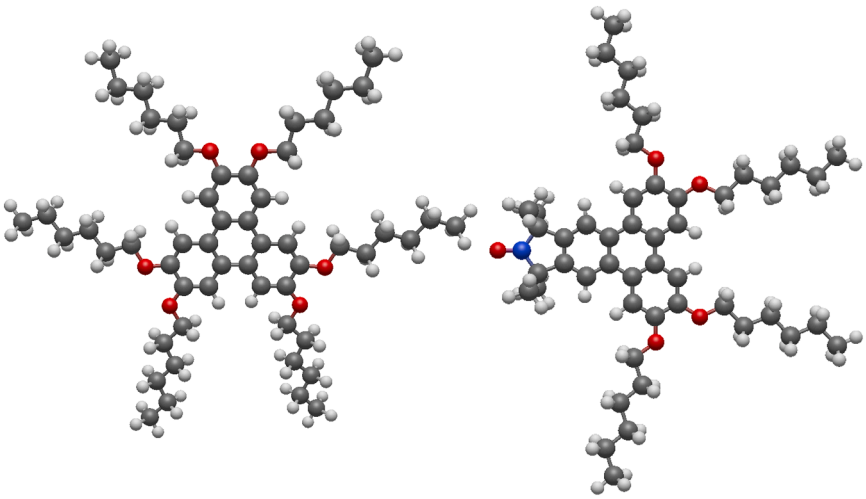

Figure 1. Structures of discotic liquid crystal molecules
HAT6 (left) and (hexyloxy)triphenylene spin probe SPN (right).

however, that both classical and machine-learned force fields are tuned primarily to the well-sampled regions of a potential energy surface, and as such are often less good at capturing dynamics, which might be strongly influenced by parts of the potential energy surface that are more rarely sampled. The same limitations may also affect force field transferability across different temperatures.

In this study, we perform atomistic molecular dynamics (MD) simulations of the 2,3,6,7,10,11 hexa(hexyloxy)triphenylene (HAT6) liquid crystal with a doped nitroxide spin probe (Figure 1) and compare the predicted EPR spectra with experimental ones at different temperatures. We demonstrate that EPR spectra are highly sensitive to subtle changes in both molecular order and motions within the columnar liquid crystal and pretransition isotropic phases. We show that this sensitivity is strong enough to serve as a stringent test for MD force fields—not only in capturing local structure but also in accurately representing dynamics, thereby allowing us to refine key force field parameters. Using this approach, we simulate the isotropic-columnar (Iso-Col) phase transition and accurately determine the corresponding transition temperature. Further, we reproduce EPR spectra in both isotropic and columnar phases directly from all-atom MD trajectories without the use of simplified models with adjustable parameters for the fitting of spectra. Finally, we identify structural changes associated with the pretransitional growth of columnar order as the system is cooled from the isotropic phase toward the liquid crystal transition.

RESULTS

Initial assessment of MD models

Considerable work has already been undertaken for the development of suitable force fields for liquid crystals. In this work, starting from the General Amber Force Field (GAFF[20]) with RESP (Restrained Electrostatic Potential) partial charges, then adding amendments from the GAFF-LCFF (Liquid Crystal Force Field) work of Boyd and Wilson,[17,19] we carried out a scan of temperatures across the phase transition, starting from both isotropic and columnar initial structures. We quickly observed that the rotational dynamics in the isotropic phase failed to reproduce the EPR spectra (as discussed below) and that the columnar phase was unstable at 370 K, just below the experimental phase transition temperature of 373 K. We therefore examined the factors most strongly influencing the model's behavior and identified three critical ones:

1 the strength of the interaction of the extended ring systems (as governed by the Lennard-Jones interactions for the aromatic carbons, $\varepsilon_{C(ar)}$),
2 the dihedral angle between the extended aromatic core and the alkoxy chains (governed by the v_2 force constant associated with the C(ar)-C(ar)-*O*-C(sp^3) dihedral, and
3 the partial charge model used.

Increasing $\varepsilon_{C(ar)}$ holds molecules together more strongly in columns, increasing the stability of the columnar phase. Increasing v_2(C(ar)-C(ar)-*O*-C(sp^3)) forces the molecule to become more planar by increasing the tendency of the chains to lie in the plane of the aromatic rings, again promoting columnar stacking. Finally, the RESP model (typically used with GAFF) has alternatively been replaced by the commonly used AM1-BCC charge model and CHelpG in some studies of liquid crystals.[15,21] While the partial charges obtained from these models are similar (see Methods S3), they were also found to significantly affect the local dynamics of disks (see discussion below). We investigated these factors through the behavior of the 7 models shown in Table 1.

Sensitivity of EPR spectra to spin probe reorientational dynamics

EPR is a particularly sensitive spectroscopic technique that can resolve molecular reorientational dynamics of the introduced paramagnetic spin probes on a sub-nanosecond timescale.[22,23] In the nitroxide-based spin probe, the paramagnetic tensors **g**, defining the interaction of the spin of the probe with the external magnetic field, and **A**, the ^{14}N nuclear hyperfine coupling to the electron spin, are both anisotropic, leading to a strong dependence of the EPR resonances on the direction of the applied magnetic field relative to the principal magnetic axes. At X-band (*ca*. 9.5 GHz), the spectrum is dominated by the anisotropic **A** tensor, resulting in three hyperfine coupling lines.[22,23] The EPR line shapes can range from three narrow lines due to averaging of the **A** tensor in the case of fast isotropic motion to broad complex asymmetric features in the case of the so-called "rigid limit." At X-band, the fast motional regime can be approximately defined by the following characteristic time[24]: $\tau_c < \hbar/|A_{zz} - A_\perp| \sim 2$ ns. A variety of shapes can be observed between these two limiting cases, depending on the ratio between the rotational

Table 1. Force field parameters used in different MD models and the corresponding values of effective rotational correlation times of the *z* magnetic axis of the spin probe τ^z_{SP} and in-plane and out-of-plane vectors of HAT6 molecules (τ^x_{LC} and τ^z_{LC}, respectively) calculated from MD simulations at 380 K

Model	Dihedral [kJ mol^{-1}]	ε (ca) [kJ mol^{-1}]	Charge model	τ^z_{SP} [ns]	τ^z_{LC} [ns]	τ^x_{LC} [ns]	*RSMD* [%]
a	11.5312	0.359824	CHelpG	12.33	20.29	7.37	1.5
b	9.5312	0.359824	CHelpG	9.52	11.07	5.13	4.1
c	13.5312	0.359824	CHelpG	38.00	28.31	10.16	3.3
d	11.5312	0.3418328 (−5%)	CHelpG	10.88	15.35	6.70	2.6
e	11.5312	0.3778152 (+5%)	CHelpG	20.26	23.52	8.07	2.2
f	11.5312	0.359824	AM1-BCC	8.32	9.12	6.28	3.1
g	11.5312	0.359824	RESP	15.63	23.04	9.82	4.9

For each model, the root-mean-square deviation (RMSD) between the predicted and experimental EPR spectrum at 380 K is also provided. Dihedral represents the v_2(C(ar)-C(ar)-C(sp^3)-O) force field term. ε (ca) represents the Lennard-Jones interaction parameter of aromatic core carbon atoms.

correlation time of the rotational dynamics of the spin probe and the hyperfine splitting and the level of motional constraint experienced by the probe, making the line shape sensitive on the timescale 0.1–100 ns.[22,23,25]

Figure 2 draws a comparison between the experimental EPR spectrum at 420 K and the one predicted from MD simulations based on the GAFF force field parameters taken from the literature.[17,19] There is a clear disagreement between the experimental and predicted spectra. In addition, Figure S1 shows EPR measurement in the absorption mode spectrum obtained from the numerical integration of the EPR spectra in Figure 2. As evident from the comparison in both figures, the predicted EPR lineshape is broader than the experimental one, indicating that the probe molecules in the MD model undergo slower rotational dynamics than observed experimentally at 420 K. Similar disagreements have been observed for other temperatures, and we also noted that the phase behavior for this model was completely wrong with the system forming a nematic phase ∼340 K instead of a columnar phase formation at ∼373 K. The EPR lineshape at 420 K is indicative of relatively fast rotational dynamics with many features partially averaged out. Nevertheless, even the predicted spectrum at 420 K is sensitive to the variation of force field parameters, as illustrated in Figure S2 for predicted spectra at both derivative and absorption modes for a range of values of the torsional parameter v_2.

Our strategy was to leverage the sensitivity of EPR lineshapes to test and refine the MD force field parameters for both HAT6 and the spin probe. To this end, we selected the EPR spectrum at 380 K, which represents unrestricted anisotropic rotational diffusion within the slow motional regime. This lineshape is particularly sensitive to rotational dynamics. At higher temperatures, the spectra reflect faster motions, resulting in more averaged-out features and thus less pronounced lineshapes. In contrast, spectra at lower temperatures exhibit characteristics of a mixture of isotropic and columnar phases.[8]

Figure 3 (as well as Figures S4A and S5A) shows comparisons between the experimental EPR spectrum at 380 K and those predicted from MD models by performing fine-tuning of the relevant force field parameters. Additionally, Figure S3 shows numerically integrated spectral lineshapes from Figure 3. The values of the force field parameters for each MD model are summarized in Table 1. In all figures, the prediction from the best MD (model a) is presented by the top red line.

Figure 3 illustrates the impact of varying the dihedral torsional force constant, v_2(C(ar)-C(ar)-*O*-C(sp^3)), on the EPR lineshape. When the value is reduced (model b), the probe's dynamics becomes faster, leading to a decrease in the effective correlation time (as given in Table 1) of the magnetic *z* axis from 12.33 ns (model a) to 9.52 ns (model b). Consequently, the predicted lineshape changes, with the end positions of the *I*z = +1 hyperfine coupling line shifting from 3,398 and 3,417 G (model a) to 3,401 and 3,415 G (model b), respectively. A noticeable narrowing of the *I*z = −1 hyperfine coupling line is also observed.

In contrast, increasing the torsional parameter v_2 (model c) produces the opposite effect. The edges of the *I*z = +1 line shift to 3,397 and 3,418 G, and the positive peak of the Iz = −1 line

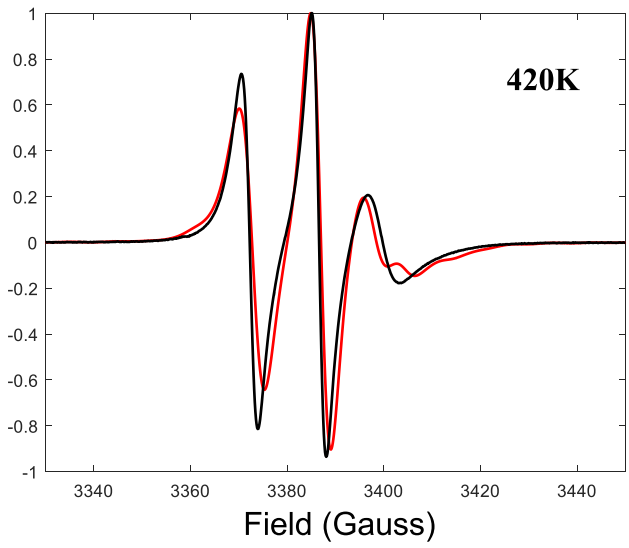

Figure 2. Initial comparison between experimental and calculated EPR spectrum of HAT6 DLC doped with nitroxide-based spin probes at 420 K

The black line is the experimental spectrum, and the red line is predicted from an MD model. Force field parameters for HAT6 are taken from the literature (GAFF/AM1-BCC). Both spectra were normalized to their maximal values.

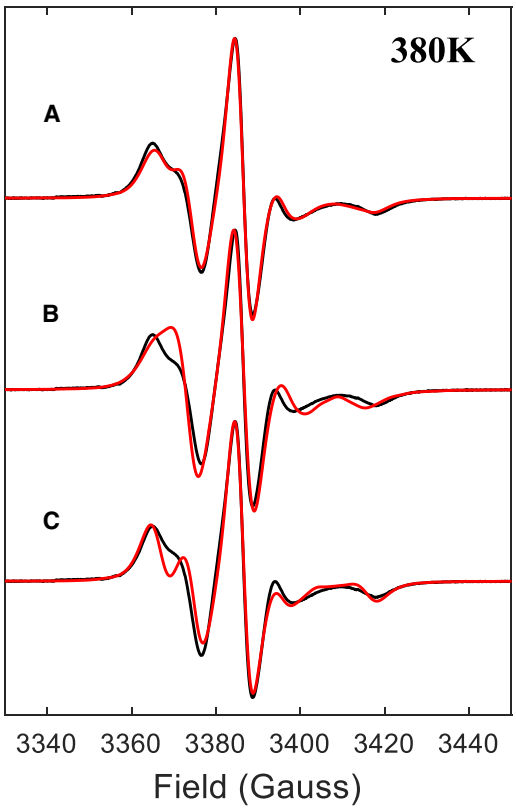

Figure 3. Comparison between the experimental EPR spectrum at 380 K and spectra predicted from different MD models

(A–C) Red lines for HAT6 DLC doped with nitroxide-based spin probes show predicted spectra from models (A), (B), and (C). These models demonstrate the significant influence of a single force-field parameter, v_2(C(ar)-C(ar)-*O*-C(sp^3)), on predicted spectra. The black lines represent the experimental EPR spectrum at 380 K. All spectra were normalized to their maximal values.

splits into two, indicating slower dynamics compared to model a. This is supported by the MD-derived effective τ^z_{SP}, which increases to 38 ns in model c. Additionally, the rotational correlation times associated with the in-plane and out-of-plane vectors *x* and *z*, respectively, of the host HAT6 molecules consistently decrease in model b and increase in model c, relative to the values from the best-fit model a. As shown in Table 1, the root-mean-square deviation (RMSD) between the predicted and experimental spectra more than doubles for models b and c compared to model a.

Similar changes in the EPR lineshape are observed when modifying the charge scheme parameters (models f and g). The predicted spectra are shown in Figure S4. Again, the RMSD increases by more than a factor of two relative to model a (see Table 1). A comparable trend is seen with variation in the ε parameter (models d and e in Figure S5), although the RMSD increase is less pronounced than in models f and g.

It is very instructive to ask why the dynamics in the isotopic phase in the temperature range 380–420 K are quite so sensitive to small elements of the force field. This is because, in this temperature range, the system is in the pretransitional region of the isotropic phase, where there is the presence of short dynamically transient molecular stacks (see below). An increase in $\varepsilon_{C(ar)}$ by 5% leads to only a small increase in system density 0.15% (at 420 K). However, the extent of pretransitional order is extremely sensitive to the proximity to the phase transition (Figure S9), which in turn is strongly influenced by system density. To examine this, we calculated the distance-dependent pairwise orientational correlation function $g_2(r)$ for each system:

$$g_2(r) = \langle P_2(\cos\theta_{ij})\rangle_{r_{ij}\in[r,r+\Delta r]}, \quad \text{(Equation 1)}$$

where $\cos\boldsymbol{\theta_{ij}} = \boldsymbol{u_i}\cdot\boldsymbol{u_i}$, for the short axis vectors $\boldsymbol{u_i}$ and $\boldsymbol{u_j}$, and the angular brackets indicate an average over all pairs of molecules whose center-center separations lie within a spherical shell of inner radius *r* and thickness Δr. Figure S9 shows how $g_2(r)$ naturally changes with temperature for model a, as the system is cooled from 420 to 380 K, reflecting the growth of short columnar stacks. Beyond an initial strong face-to-face pairing between two molecules, we appear to get an exponential decay of stack lengths that can be fitted by a single exponential decay between 7 and 20 Å (Figure S13). The correlation length ξ associated with this fit is given in Table S5 and is closely related to the changes in the reorientational time noted above. Increasing $\varepsilon_{C(ar)}$ leads to a slightly longer decay in $g_2(r)$ arising from an increase in stack length (Figure S12) and a larger value for ξ.

Similarly, the charge models (Figure S11; Table S5), demonstrate a difference in transient molecular face-to-face stacking, with the CHelpG charge distribution leading to the strongest stacking, and the smaller magnitude charges obtained for AM1-BCC (which is the charge distribution most often used with GAFF), leading to considerably weaker stacking at 420 K. Finally, the dihedral behavior noted in Figure S2 (along with the corresponding $g_2(r)$ in Figure S10) is very subtle. Higher values of v_2(C(ar)-C(ar)-*O*-C(sp^3)) lead to alkoxy chains lying more in the plane of the extended aromatic ring. This enhances stacking behavior, leading to slower dynamics in the isotropic phase (Figure S10; Table S5).

We note in passing that increasing v_2(C(ar)-C(ar)-*O*-C(sp^3)) for the original GAFF force field with AM1-BCC charges will allow for the stabilization of a columnar phase with a phase transition to an isotropic phase in the region 360–380 K. However, here the local stacking of discs is unphysically increased, resulting in a dramatic slowing of the dynamics (see Methods S6). This failure is clearly seen in the disagreement between predicted and experimental EPR spectra in Figure S15.

Final force field parameters and predicted EPR spectra at different temperatures

The force field parameters obtained through fine-tuning using the EPR spectrum at 380 K were independently applied to predict the spectra at three characteristic additional temperatures across the Iso-Col phase transition. The results are presented in Figure 4. A comparison between predicted and experimental spectra in absorption mode is provided in Figure S6.

The autocorrelation functions of the magnetic *z* axis of (hexyloxy)triphenylene nitroxide-based spin probe analog (SPN) at different temperatures, calculated from MD simulations using Equation 2 (see the methods section), are shown in Figure 5. These functions were fitted using Equation 4, which accounts for two contributions to the reorientational dynamics of the

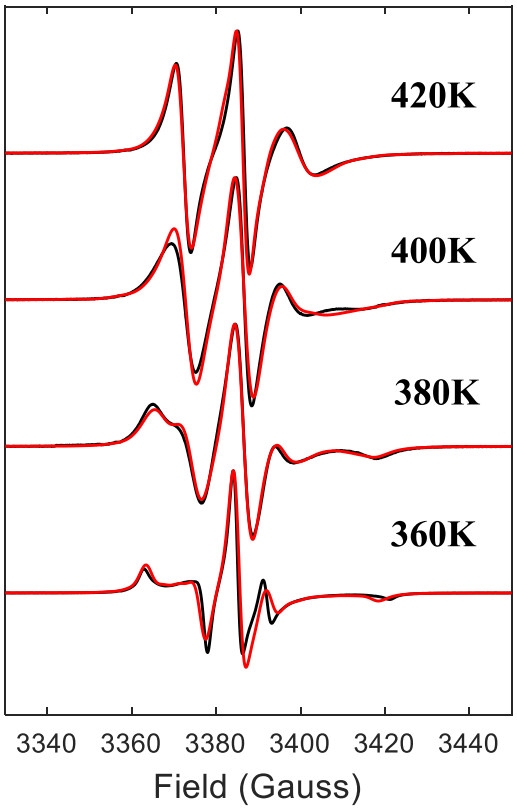

Figure 4. Comparison between the best predicted MD spectra and experimental spectra at different temperatures

MD model (red lines) and experimental (black lines) EPR spectra of HAT6 DLC doped with nitroxide-based spin probe at different temperatures. All spectra were normalized to their maximal values.

spin probe. The fitted parameters corresponding to fast (local) and slow (global) motional components of the nitroxide group, along with the effective correlation times calculated using Equation 5, are summarized in Table S1. Additionally, the MD-derived effective rotational correlation times for the molecular vectors *x* and *z* of the HAT6 core using Equations 2 and 4, as well as the order parameters of both SPN and HAT6 molecules (in the laboratory fixed frame), are presented in Table 2.

The results demonstrate excellent agreement with the experimental spectra, capturing all characteristic features of the lineshapes across the temperature range. The lineshape at 420 K, indicative of partially averaged rotational dynamics, undergoes progressive broadening as the temperature decreases. The correlation times τ^z_{SP}, calculated from MD simulations, are broadly consistent with previously reported values for SPN doped in HAT6, obtained from the fitting of EPR spectra using the Brownian dynamics (BD) simulation model for rigid-body anisotropic rotational diffusion.[8] For instance, the reported adjusted effective correlation times τ^z_{SP} at 420, 399, 378, and 360 K were 6.22, 9.77, 16.10, and 15.32 ns, respectively—values that are comparable to those listed in Table 2 for the closest corresponding temperatures. However, importantly, the MD-predicted spectra in this work show far better agreement with experiment than those obtained using the BD rigid-rod model.[8] This improvement is attributed to the more realistic representation of MD in atomistic MD simulations compared to the simplified BD approach.

Order in the columnar phase

Snapshots from the phases are shown in Figure 6. At 360 K, our MD simulations predict the formation of the columnar phase (see snapshots in Figures 6B and 6C), in agreement with experimental observations. The uniaxial order parameter from the best model (model a) is plotted in Figure 7 for 360 and 380 K. Here, we plot the system order parameter S^a_2 defined from the central short axes of all molecules (S^a_2; see Methods S2). At 360 K, we get a well-ordered columnar system, whereas at 380 K, we see decay of the orientational order, which occurs very slowly over 400 ns, followed by strong pretransitional fluctuations over another 500 ns.

Figure 6B shows the typically disordered columns that we expect to see in a columnar phase. These arise from thermal motion leading to dynamic disorder in both stacking distances and orientations. This is believed to lead to most columnar liquid crystals exhibiting hopping transport, rather than behaving as truly delocalized 1D conductors (which could potentially arise from strongly 1D-ordered aromatic ring systems).[26–28] Figure 6D shows a top view looking down the columnar director. The spin probes are shown in colored space-filling representation, demonstrating that they are localized into columns, but a part of the spin probe often sits slightly outside the column cross-section. This is to be expected as the aromatic core of the spin probe is not perfectly matched to the triphenylene core of HAT6. Nonetheless, comparison of the spin probe and system order parameters in Methods S2 shows that the spin probe provides an excellent representation of the system's overall order. The spectrum at 360 K predicted from MD is shown as the red bottom line in Figure 4. It broadly agrees with the experimental spectrum, reproducing all major features except for some narrowing of the hyperfine coupling lines that suggests increased mobility of the spin probe, likely due to tilt motions of the nitroxide ring. This small discrepancy between the MD-predicted and experimentally measured spectra is related to the packing behavior of DLC molecules under the influence of the external magnetic field used in the spectrometer.[8]

As previously discussed, molecular alignment in DLCs occurs in macroscopic domains. Due to the large diamagnetic anisotropy of the polyaromatic core in most DLCs, including HAT6, the director (perpendicular to the aromatic planes and aligned along the column axis) tends to orient perpendicular to the applied magnetic field.[29] In the columnar phase, the resonant magnetic field of a $g = 2$ paramagnet at X band (~3,400 G) induces partial alignment of HAT6 columns perpendicular to the field direction, as schematically shown in Figure S14. The effects of columnar director distribution were modeled using a simple Gaussian distribution function of the orientations of the director's vector relative to the external magnetic field, with the mean orientation angle and distribution bandwidth of 90° and 45°, respectively. Importantly, the magnetic field also stabilizes columnar packing, thereby reducing the rotational flexibility of both the spin probes and the host HAT6 molecules. Indeed, our previous results using the BD simulation model for

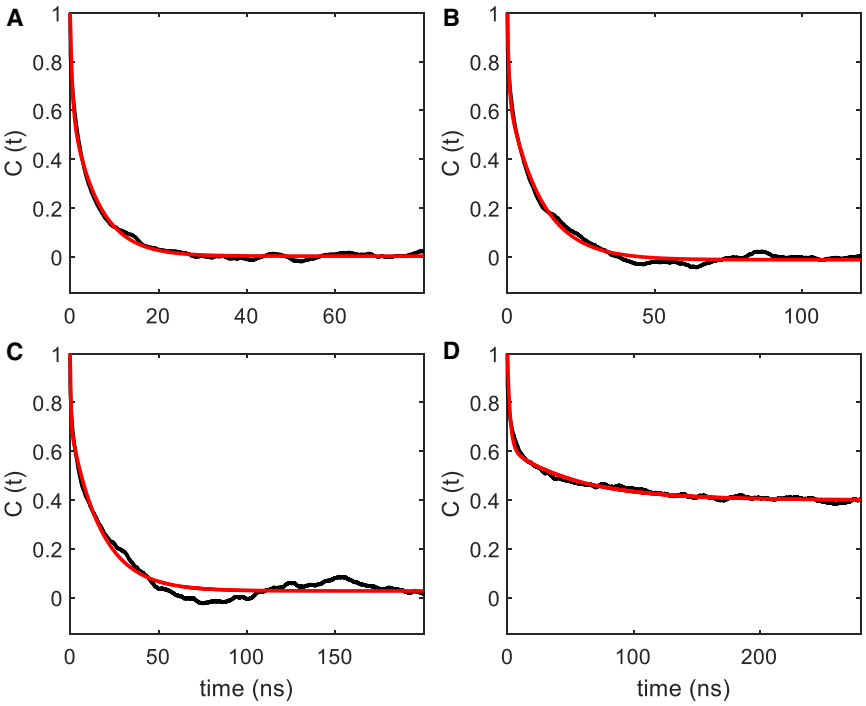

Figure 5. Autocorrelation functions of the *z* magnetic axis of the spin probe

(A), (B), (C), and (D) correspond to 420, 400, 380, and 360 K, respectively. Autocorrelation functions calculated from MD trajectories using Equation 2 and their bi-exponential fittings using Equation 4 are shown by black and red lines, respectively.

rotational diffusion of the spin probe in the presence of a restoring potential[8,22,23] showed that an order parameter of 0.82 was required to achieve a good fit to the experimental spectrum at 360 K. However, the value calculated from the columnar phase simulated in this work is lower, 0.63 (in the laboratory fixed frame), which explains the noticeable difference in the outer peak position of the *Iz* = +1 hyperfine coupling line observed between the predicted and experimental spectra around 3420 G (see Figure 4).

We note in passing that the combination of EPR with molecular simulation is far more sensitive to changes in dynamics than other techniques that probe molecular motion. Previous studies using QENS suggest that motions are little changed on moving from the columnar to the pretransitional isotropic phase.[5] Though this same QENS study concludes, as we do here, that the small amplitude in-plane motions (leading to the movement of disks over each other) are almost entirely determined by tail/tail interactions and that these interactions additionally play an important role in determining the out-of-plane motion.

Table 2. Effective rotational correlation times and order parameters of SPN and HAT6 host molecules at different temperatures

T [K]	τ^z_{SP} [ns][a]	τ^z_{LC} [ns]	τ^x_{LC} [ns]	S_{SP}	S_{LC}
420	3.97	4.94	2.20	0	0
400	7.70	10.35	4.11	0	0
380	12.33	20.29	7.37	0	0
360	20.87	18.90	5.37	0.63	0.65

[a]Order parameters here are calculated in the laboratory fixed frame.

DISCUSSION

Overall, the results demonstrate that EPR spectra are highly sensitive to subtle changes in both molecular order and dynamical motion within the columnar liquid crystal phase of HAT6 and its pretransitional isotropic phase. This sensitivity provides a stringent test for MD force fields. Small changes in the force field—such as the charge model, the Lennard-Jones interactions of the aromatic core, and the magnitude of the energy barrier associated with a key torsional angle (C(ar)–C(ar)–O–C(sp^3))—lead to significant alterations in local structure and dynamics. Remarkably, these effects are observed even in the isotropic phase, where changes in these parameters result in substantial changes to the EPR line shape. Importantly, these variations lie well within the typical uncertainties associated with force field parameterization. EPR spectroscopy with spin probes, therefore, emerges as an ultra-sensitive approach for evaluating whether a force field can accurately capture not just equilibrium structure, but also the underlying dynamics—that is, the trajectory through the free energy landscape.

Using our fine-tuned model, we can directly reproduce EPR spectra across a temperature range in the pretransitional region of the isotropic phase, capturing in the process subtle changes in molecular order that could not be predicted from empirical modeling of the EPR spectra. Our same force field reproduces the columnar-isotropic phase transition and, in addition, successfully predicts the EPR spectrum in the columnar phase.

METHODS

MD simulations

Atomistic MD simulations were conducted on the columnar liquid crystal molecule HAT6 and the purpose-designed nitroxide-based spin probe, previously reported in the literature,[8] whose structures are given in Figure 1. HAT6 is a classic triphenylene DLC molecule that exhibits a hexagonal columnar phase (Colh) and has been widely studied for its charge transport properties and self-assembly behavior.

The GROMACS[30,31] 2023.1 package was used to carry out all MD simulations using a classical force field. As a starting point, the simulations made use of the GAFF[20] parameter set using the GAFF-LCFF amendments due to Boyd and Wilson.[17,19,32,33] These have been shown to provide a good prediction of

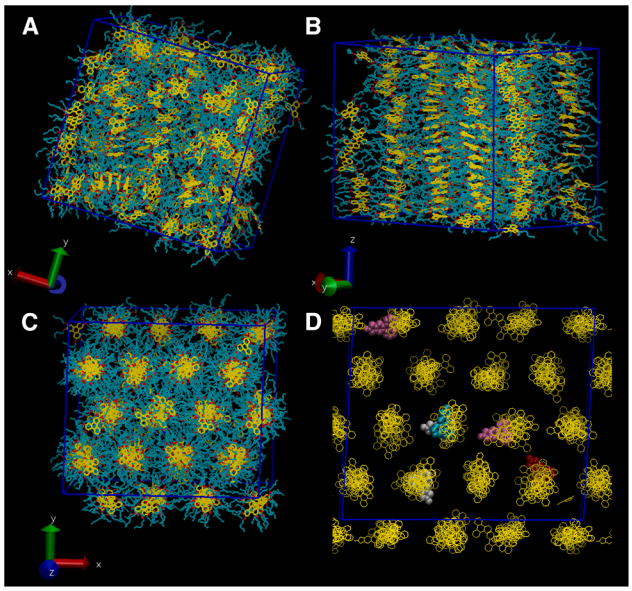

Figure 6. Snapshots showing the structure of the phases obtained

(A) Isotropic phase at 420 K showing some pretransitional ordering of aromatic cores.

(B) Columnar phase at 360 K (side view).

(C) Columnar phase at 360 K (viewed from above the columns).

(D) Aromatic cores showing the position of spin probes.

Aromatic cores are shown in yellow, chains are shown in blue, and hydrogens are not shown.

transition temperatures for a nematic.[17] Here, the interaction potential takes the usual form[17,34] and the standard Lorentz-Berthelot mixing rules are applied throughout. The Antechamber software from AmberTools was used to generate GAFF force fields. We explored three standard charge models, AM1-BCC,[35,36] RESP,[37] and CHelpG.[38] The GAFF topologies and coordinate files obtained from Antechamber were converted into the GROMACS format using the ACPYPE script.[39] For the spin probe head group, bond lengths and angles were tuned to reproduce results from density functional theory (DFT) (B3LYP functional) calculations. The original GAFF improper dihedral force constants that enforce planarity in ring structures (and a degree of rigidity with respect to out-of-plane bends) are represented by proper dihedrals within the GROMACS force field. For these, the original GAFF force constants are known to be small (in comparison to other force fields), and are less appropriate for extended ring structures than for benzene. Consequently, these were increased from 4.6 to 10 kJ mol^{-1}[40,41] for both HAT6 and SPN. The results section considers the sensitivity of the simulated structures to changes in the charge model, the Lennard-Jones interactions of the aromatic core, and the magnitude of the energy barrier associated with a key torsional angle (C(ar)–C(ar)–O–C(sp^3)) that controls the planarity of the hexyloxy chains. The different models used are summarized in Table 1. Force field parameters are provided (see Methods S6).

Calculations were started from pre-assembled hexagonally columnar phases (304 molecules in 16 columns) and from randomly distributed and orientated molecules (300 molecules), initially at low density but compressed to liquid-state densities during a multi-step equilibration procedure (as used for previous liquid crystalline systems).[40,41] Production runs were conducted in the constant-*NpT* ensemble at a range of temperatures using a Nosé-Hoover thermostat with pressure controlled using a Parrinello-Rahman barostat at atmospheric pressure, with isotropic pressure coupling for the isotopic phase and anisotropic pressure coupling for the liquid crystal phase. Bond constraints were applied to hydrogens using the LINCS algorithm with a 2 femtosecond (fs) time step. Interaction cutoffs were applied for Lennard-Jones (1.2 nm) and Coulombic interactions (1.2 nm). The long-range part of the Coulomb potential was accounted for by employing a particle mesh Ewald (PME) method. Lengths of production runs were as stated below (but typically 300–700 ns for liquid crystal phases and 200 ns for the isotropic liquid phase), with sampling of coordinate sets carried out at 80 picosecond (ps) intervals.

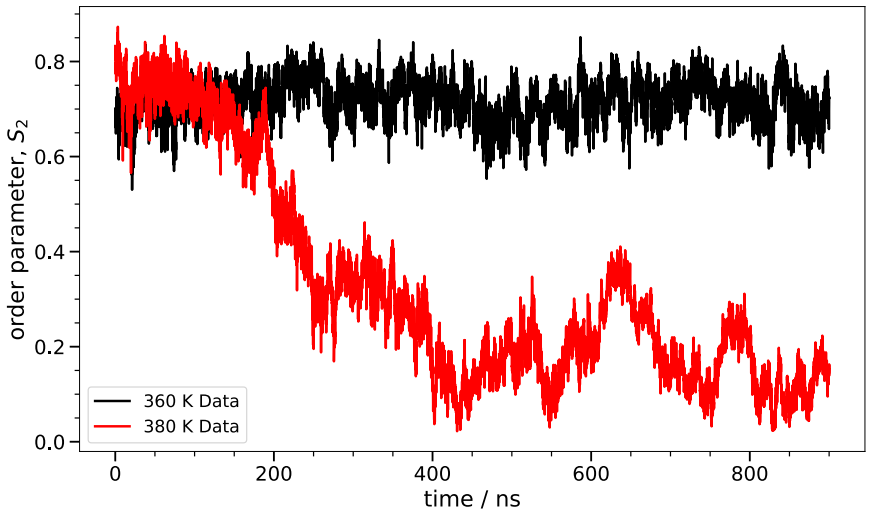

Figure 7. Uniaxial order parameter vs. time for the optimized discotic model at 360 and 380 K

Here, order parameters are measured as the system order parameters based on the central short axis of each molecule, S_2^3 (see Methods S2), calculated relative to the local instantaneous director for every simulation snapshot.

Prediction of EPR spectra from MD trajectories

A trajectory-based method that employs the numerical solution of the stochastic Liouville equation (SLE) in the Langevin form for the spin density matrix has been used for the simulation of the EPR line shapes.[22–24,42,43] An MD-EPR simulation methodology, developed and described previously by one of us,[44] has been employed in this work. According to this approach, a numerical initial propagation of the density matrix is required only until the point in time when the autocorrelation function of the re-orientational motion of the spin probe has completely relaxed, $t \sim 10\tau_c$, where τ_c is the effective correlation time of the motion.[44] The evolution of the spin density matrix for the remaining working length can then be predicted from the MD data using well-defined parameters (see Methods S1 for full details). This methodology has been successfully applied to various complex molecular systems, including proteins, lyotropic mesophases, DNA fragments, lipid membranes, and also to liquid crystals.[22,44–47] The main advantage of such an approach is that it allows predictions of EPR spectra from relatively short MD trajectories, up to the point when autocorrelation functions of rotational dynamics are fully relaxed. In all simulations in the present study, concatenated MD trajectories obtained from the multiple probes in the system have been used.

The EPR spectral line shapes of nitroxide spin probes are determined entirely by the variation in time of two angles that define the orientation of the applied magnetic field to the principal axis of the nitroxide group. Therefore, the orientational history of the magnetic axes in the fixed frame of the simulation box is calculated and processed. The z axis of the nitroxide ring (coincident with the direction of p_z-orbital of N) is calculated from the cross-product of the unit vectors of the two N–C bonds of the ring (see Figure S7). The x axis is calculated as a projection vector of the N–O bond on the nitroxide plane (defined by the C–N–C atoms), and the y axis is taken as a cross-product of the z and x vectors. The following principal values of the **g** and **A** hyperfine coupling tensors of the spin probe, obtained from DFT calculations and reported previously, have been employed: $g_{xx} = 2.0081$, $g_{yy} = 2.0060$, $g_{zz} = 2.0022$, $A_{xx} = 5.4$ G, $A_{yy} = 5.3$ G, and $A_{zz} = 31.5$ G.[8]

Details of the variable temperature CW EPR measurements on HAT6 have been reported previously and are provided in the supplemental information.

Rotational autocorrelation functions and calculation of effective rotational correlation times

The autocorrelation function of a selected vector $\vec{l}$ (e.g., z magnetic axis of the spin probe) were calculated from MD trajectories according to the following expression[14,48]:

$$C_l(t) = \left\langle \int_0^\infty P_2\left(\vec{l}(\tau)\cdot\vec{l}(t+\tau)\right)d\tau \right\rangle, \qquad \text{(Equation 2)}$$

where $P_2(x)$ is the second-order Legendre polynomial:

$$P_2(x) = \frac{1}{2}\left(3x^2 - 1\right), \qquad \text{(Equation 3)}$$

and the triangular brackets denote the average taken over time and the number of molecules involved in each case. A "sliding time window" approach was used for time averaging.[44] The autocorrelation functions for molecules in oriented media are characterized by two distinct motional contributions. The fast decay is attributed to the local rotational motions of both spin probes and host molecules.[14,45,49] The slow decay is associated with reorientation motion of the restricted local environment of these molecules. Effective rotational correlation times of the selected vectors were obtained from the results of bi-exponential fitting of the respective autocorrelation functions using the following equation:

$$C_l(t) = \left(1 - S_0^2\right)\left(w_1 \exp\left(-\frac{t}{\tau_1}\right) + w_2 \exp\left(-\frac{t}{\tau_2}\right)\right) + S_0^2, \qquad \text{(Equation 4)}$$

where τ_1 and τ_2 are correlation times of the fast and slow motional contributions, respectively, with associated weights w_i, and S_0^2 is the square of the generalized order parameter S_0, noting that $S_0^2 = C_l(\infty)$. The effective correlation time τ_{eff} represents an average of the individual motional contributions, each associated with a specific correlation time τ_i and a weight w_i. The following relationship holds between τ_{eff} and τ_1 and τ_2:

$$\tau_{eff} = \frac{\int_0^\infty \left(C_l(t) - C_l(\infty)\right)dt}{1 - C_l(\infty)} = w_1\tau_1 + w_1\tau_2. \qquad \text{(Equation 5)}$$

Molecular vectors x and z (in-plane and out-of-plane, respectively) for each HAT6 molecule are defined using relevant atoms of the core (see Figure S7). Based on atomic positions, we can also calculate order parameters for each HAT6 molecule (see Methods S2). In addition, in Table 2, we quote order parameters based on fitting of the autocorrelation function for the z (out-of-plane) vector of the HAT6 core (see Methods S1).

RESOURCE AVAILABILITY

Lead contact

Requests for further information and resources should be directed to and will be fulfilled by the lead contact, Mark Richard Wilson (mark.wilson@durham.ac.uk).

Materials availability

This study did not generate new, unique reagents.

Data and code availability

- All data reported in this paper will be shared by the lead contact upon request. Our supporting research dataset is published in the Durham University Research Data Repository. DOI: http://doi.org/10.15128/r1cc08hf71v.
- This paper does not report original code.
- Any additional information required to reanalyze the data reported in this paper is available from the lead contact upon request.

ACKNOWLEDGMENTS

The authors would like to thank Durham University for providing computer time on its high-performance computer (HPC) system Hamilton8 and the Research Computing Service at the University of East Anglia for access to the HPC cluster, Ada. This work also made use of the HPC system Bede at the N8 Centre of Excellence in Computationally Intensive Research (N8 CIR) provided and funded by the N8 research partnership and EPSRC (grant no. EP/T022167/1). The center is coordinated by the Universities of Durham, Manchester,

and York. The authors thank the EPSRC for funding through grants EP/L001322/1 and EP/L00111X/1.

AUTHOR CONTRIBUTIONS

Conceptualization, data curation, formal analysis, funding acquisition, investigation, methodology, project administration, software, validation, visualization, writing – original draft, and writing – review and editing: M.R.W. and V.S.O.

DECLARATION OF INTERESTS

The authors declare no competing interests.

SUPPLEMENTAL INFORMATION

Supplemental information can be found online at https://doi.org/10.1016/j.xcrp.2026.103332.

Received: January 28, 2026
Revised: March 20, 2026
Accepted: April 30, 2026
Published: May 29, 2026

REFERENCES

1. Wöhrle, T., Wurzbach, I., Kirres, J., Kostidou, A., Kapernaum, N., Litterscheidt, J., Haenle, J.C., Staffeld, P., Baro, A., Giesselmann, F., and Laschat, S. (2016). Discotic Liquid Crystals. Chem. Rev. *116*, 1139–1241. https://doi.org/10.1021/acs.chemrev.5b00190.
2. Schmidt-Mende, L., Fechtenkötter, A., Müllen, K., Moons, E., Friend, R.H., and MacKenzie, J.D. (2001). Self-organized discotic liquid crystals for high-efficiency organic photovoltaics. Science *293*, 1119–1122. https://doi.org/10.1126/science.293.5532.1119.
3. Lamarra, M., Muccioli, L., Orlandi, S., and Zannoni, C. (2012). Temperature dependence of charge mobility in model discotic liquid crystals. Phys. Chem. Chem. Phys. *14*, 5368–5375. https://doi.org/10.1039/c2cp23178f.
4. Andrienko, D., Marcon, V., and Kremer, K. (2006). Atomistic simulation of structure and dynamics of columnar phases of hexabenzocoronene derivatives. J. Chem. Phys. *125*, 124902. https://doi.org/10.1063/1.2354156.
5. Mulder, F.M., Stride, J., Picken, S.J., Kouwer, P.H.J., De Haas, M.P., Siebbeles, L.D.A., and Kearley, G.J. (2003). Dynamics of a triphenylene discotic molecule, HAT6, in the columnar and isotropic liquid phases. J. Am. Chem. Soc. *125*, 3860–3866. https://doi.org/10.1021/ja029227f.
6. Haverkate, L.A., Zbiri, M., Johnson, M.R., Deme, B., Mulder, F.M., and Kearley, G.J. (2011). Conformation, defects, and dynamics of a discotic liquid crystal and their influence on charge transport. J. Phys. Chem. B *115*, 13809–13816. https://doi.org/10.1021/jp2068478.
7. Haverkate, L.A., Zbiri, M., Johnson, M.R., Deme, B., Mulder, F.M., and Kearley, G.J. (2012). Erratum: Conformation, defects, and dynamics of a discotic liquid crystal and their influence on charge transport. J. Phys. Chem. B *116*, 3908. https://doi.org/10.1021/JP3017562.
8. Gopee, H., Cammidge, A.N., and Oganesyan, V.S. (2013). Probing Columnar Discotic Liquid Crystals by EPR Spectroscopy with a Rigid-Core Nitroxide Spin Probe. Angew. Chem. Int. Ed. *52*, 8917–8920. https://doi.org/10.1002/ANIE.201303194.
9. Muccioli, L., Berardi, R., Orlandi, S., Ricci, M., and Zannoni, C. (2007). Molecular properties and stacking of 1-substituted hexaalkoxy triphenylenes. Theor. Chem. Acc. *117*, 1085–1092. https://doi.org/10.1007/s00214-006-0229-7.
10. Orlandi, S., Muccioli, L., Ricci, M., Berardi, R., and Zannoni, C. (2007). Core charge distribution and self assembly of columnar phases: the case of triphenylenes and azatriphenylenes. Chem. Cent. J. *1*, 15. https://doi.org/10.1186/1752-153X-1-15.
11. Camerel, F., Barrière, F., and Jeannin, O. (2018). Simulation of SAXS patterns of hexa-n-alkoxy-2,3,6,7,10,11-triphenylene mesophase. Liq. Cryst. *45*, 698–702. https://doi.org/10.1080/02678292.2017.1376124.
12. Olivier, Y., Muccioli, L., Lemaur, V., Geerts, Y.H., Zannoni, C., and Cornil, J. (2009). Theoretical Characterization of the Structural and Hole Transport Dynamics in Liquid-Crystalline Phthalocyanine Stacks. J. Phys. Chem. B *113*, 14102–14111. https://doi.org/10.1021/jp9061169.
13. Zhu, R., Yan, T., Wang, Y., and Saielli, G. (2025). Towards quantitative prediction of proton chemical shifts in imidazolium chloride ionic liquids by computational NMR. Phys. Chem. Chem. Phys. *27*, 25310–25321. https://doi.org/10.1039/d5cp03322e.
14. Catte, A., White, G.F., Wilson, M.R., and Oganesyan, V.S. (2018). Direct Prediction of EPR Spectra from Lipid Bilayers: Understanding Structure and Dynamics in Biological Membranes. ChemPhysChem *19*, 2183–2193. https://doi.org/10.1002/CPHC.201800386.
15. Chami, F., Wilson, M.R., and Oganesyan, V.S. (2012). Molecular dynamics and EPR spectroscopic studies of 8CB liquid crystal. Soft Matter *8*, 6823–6833. https://doi.org/10.1039/C2SM25429H.
16. Erastova, V., Evans, I.R., Glossop, W.N., Guryel, S., Hodgkinson, P., Kerr, H.E., Oganesyan, V.S., Softley, L.K., Wickins, H.M., and Wilson, M.R. (2024). Unravelling Guest Dynamics in Crystalline Molecular Organics Using ^{2}H Solid-State NMR and Molecular Dynamics Simulation. J. Am. Chem. Soc. *146*, 18360–18369. https://doi.org/10.1021/jacs.4c03246.
17. Boyd, N.J., and Wilson, M.R. (2015). Optimization of the GAFF force field to describe liquid crystal molecules: the path to a dramatic improvement in transition temperature predictions. Phys. Chem. Chem. Phys. *17*, 24851–24865. https://doi.org/10.1039/C5CP03702F.
18. Jin, Y., Perez-Lemus, G.R., Zubieta Rico, P.F., and de Pablo, J.J. (2024). Improving Machine Learned Force Fields for Complex Fluids through Enhanced Sampling: A Liquid Crystal Case Study. J. Phys. Chem. A *128*, 7257–7268. https://doi.org/10.1021/acs.jpca.4c01546.
19. Boyd, N.J., and Wilson, M.R. (2018). Validating an optimized GAFF force field for liquid crystals: T_{NI} predictions for bent-core mesogens and the first atomistic predictions of a dark conglomerate phase. Phys. Chem. Chem. Phys. *20*, 1485–1496. https://doi.org/10.1039/C7CP07496D.
20. Wang, J., Wolf, R.M., Caldwell, J.W., Kollman, P.A., and Case, D.A. (2004). Development and testing of a general Amber force field. J. Comput. Chem. *25*, 1157–1174. https://doi.org/10.1002/jcc.20035.
21. Chami, F., and Wilson, M.R. (2010). Molecular order in a chromonic liquid crystal: A molecular simulation study of the anionic azo dye sunset yellow. J. Am. Chem. Soc. *132*, 7794–7802. https://doi.org/10.1021/ja102468g.
22. Oganesyan, V.S. (2018). EPR spectroscopy and molecular dynamics modelling: a combined approach to study liquid crystals. Liq. Cryst. *45*, 2139–2157. https://doi.org/10.1080/02678292.2018.1508767.
23. Oganesyan, V.S. (2014). Computational approaches for simulating motional EPR spectra. In SPR: Electron Paramagnetic Resonance, *24*, B. Gilbert, V. Chechik, and D.M. Murphy, eds. (Royal Society of Chemistry), pp. 32–61.
24. Steinhoff, H.J., and Hubbell, W.L. (1996). Calculation of electron paramagnetic resonance spectra from brownian dynamics trajectories: application to nitroxide side chains in proteins. Biophys. J. *71*, 2201–2212. https://doi.org/10.1016/S0006-3495(96)79421-3.
25. Catte, A., Wilson, M.R., Walker, M., and Oganesyan, V.S. (2018). Antimicrobial action of the cationic peptide, chrysophsin-3: a coarse-grained molecular dynamics study. Soft Matter *14*, 2796–2807. https://doi.org/10.1039/C7SM02152F.
26. Kirkpatrick, J., Marcon, V., Nelson, J., Kremer, K., and Andrienko, D. (2007). Charge mobility of discotic mesophases: A multiscale quantum and classical study. Phys. Rev. Lett. *98*, 227402. https://doi.org/10.1103/PhysRevLett.98.227402.
27. Rühle, V., Lukyanov, A., May, F., Schrader, M., Vehoff, T., Kirkpatrick, J., Baumeier, B., and Andrienko, D. (2011). Microscopic simulations of charge

transport in disordered organic semiconductors. J. Chem. Theory Comput. *7*, 3335–3345. https://doi.org/10.1021/CT200388S.

28. Feng, X., Marcon, V., Pisula, W., Hansen, M.R., Kirkpatrick, J., Grozema, F., Andrienko, D., Kremer, K., and Müllen, K. (2009). Towards high charge-carrier mobilities by rational design of the shape and periphery of discotics. Nat. Mater. *8*, 421–426. https://doi.org/10.1038/nmat2427.
29. Lee, J.H., Choi, S.M., Pate, B.D., Chisholm, M.H., and Han, Y.S. (2006). Magnetic uniaxial alignment of the columnar superstructure of discotic metallomesogens over the centimetre length scale. J. Mater. Chem. *16*, 2785. https://doi.org/10.1039/b603902b.
30. Abraham, M.J., Murtola, T., Schulz, R., Páll, S., Smith, J.C., Hess, B., and Lindahl, E. (2015). Gromacs: High performance molecular simulations through multi-level parallelism from laptops to supercomputers. SoftwareX *1–2*, 19–25. https://doi.org/10.1016/j.softx.2015.06.001.
31. Pronk, S., Páll, S., Schulz, R., Larsson, P., Bjelkmar, P., Apostolov, R., Shirts, M.R., Smith, J.C., Kasson, P.M., van der Spoel, D., et al. (2013). {GROMACS} 4.5: a high-throughput and highly parallel open source molecular simulation toolkit. Bioinformatics *29*, 845–854. https://doi.org/10.1093/bioinformatics/btt055.
32. Shadpour, S., Nemati, A., Boyd, N.J., Li, L., Prévôt, M.E., Wakerlin, S.L., Vanegas, J.P., Salamończyk, M., Hegmann, E., Zhu, C., et al. (2019). Heliconical-layered nanocylinders (HLNCs)-hierarchical self-assembly in a unique B4 phase liquid crystal morphology. Mater. Horiz. *6*, 959–968. https://doi.org/10.1039/c9mh00089e.
33. Shadpour, S., Nemati, A., Salamończyk, M., Prévôt, M.E., Liu, J., Boyd, N.J., Wilson, M.R., Zhu, C., Hegmann, E., Jákli, A.I., et al. (2020). Missing Link between Helical Nano- and Microfilaments in B4 Phase Bent-Core Liquid Crystals, and Deciphering which Chiral Center Controls the Filament Handedness. Small *16*, e1905591. https://doi.org/10.1002/smll.201905591.
34. Thind, R., Walker, M., and Wilson, M.R. (2018). Molecular Simulation Studies of Cyanine-Based Chromonic Mesogens: Spontaneous Symmetry Breaking to Form Chiral Aggregates and the Formation of a Novel Lamellar Structure. Adv. Theory Simul. *1*, 1800088. https://doi.org/10.1002/adts.201800088.
35. Jakalian, A., Bush, B.L., Jack, D.B., and Bayly, C.I. (2000). Fast, Efficient Generation of High-Quality Atomic Charges. AM1-BCC Model: I. Method. J. Comput. Chem. *21*, 132–146. https://doi.org/10.1002/(SICI)1096-987X(20000130)21:2.
36. Jakalian, A., Jack, D.B., and Bayly, C.I. (2002). Fast, efficient generation of high-quality atomic charges. AM1-BCC model: II. Parameterization and validation. J. Comput. Chem. *23*, 1623–1641. https://doi.org/10.1002/JCC.10128.
37. Bayly, C.I., Cieplak, P., Cornell, W., and Kollman, P.A. (1993). A Well-Behaved Electrostatic Potential Based Method Using Charge Restraints for Deriving Atomic Charges: The RESP Model. J. Phys. Chem. *97*, 10269–10280. https://doi.org/10.1021/j100142a004.
38. Breneman, C.M., and Wiberg, K.B. (1990). Determining atom-centered monopoles from molecular electrostatic potentials. The need for high sampling density in formamide conformational analysis. J. Comput. Chem. *11*, 361–373. https://doi.org/10.1002/JCC.540110311.
39. da Silva, A.W., and Vranken, W.F. (2012). ACPYPE - AnteChamber PYthon Parser interfacE. BMC Res. Notes *5*, 367. https://doi.org/10.1186/1756-0500-5-367.
40. Yu, G., Walker, M., and Wilson, M.R. (2021). Atomistic simulation studies of ionic cyanine dyes: self-assembly and aggregate formation in aqueous solution. Phys. Chem. Chem. Phys. *23*, 6408–6421. https://doi.org/10.1039/D0CP06205G.
41. Yu, G., and Wilson, M.R. (2022). All-atom simulations of bent liquid crystal dimers: the twist-bend nematic phase and insights into conformational chirality. Soft Matter *18*, 3087–3096. https://doi.org/10.1039/D2SM00291D.
42. Desensi, S.C., Rangel, D.P., Beth, A.H., Lybrand, T.P., and Hustedt, E.J. (2008). Simulation of nitroxide electron paramagnetic resonance spectra from Brownian trajectories and molecular dynamics simulations. Biophys. J. *94*, 3798–3809. https://doi.org/10.1529/biophysj.107.125419.
43. Sezer, D., Freed, J.H., and Roux, B. (2008). Parametrization, Molecular Dynamics Simulation, and Calculation of Electron Spin Resonance Spectra of a Nitroxide Spin Label on a Polyalanine α-Helix. J. Phys. Chem. B *112*, 5755–5767. https://doi.org/10.1021/jp711375x.
44. Oganesyan, V.S. (2011). A general approach for prediction of motional EPR spectra from Molecular Dynamics (MD) simulations: Application to spin labelled protein. Phys. Chem. Chem. Phys. *13*, 4724–4737. https://doi.org/10.1039/c0cp01068e.
45. Prior, C., and Oganesyan, V.S. (2017). Prediction of EPR Spectra of Lyotropic Liquid Crystals using a Combination of Molecular Dynamics Simulations and the Model-Free Approach. Chemistry (Easton). *23*, 13192–13204. https://doi.org/10.1002/chem.201702682.
46. Prior, C., Danilāne, L., and Oganesyan, V.S. (2018). All-atom molecular dynamics simulations of spin labelled double and single-strand DNA for EPR studies. Phys. Chem. Chem. Phys. *20*, 13461–13472. https://doi.org/10.1039/C7CP08625C.
47. Oganesyan, V.S., Chami, F., White, G.F., and Thomson, A.J. (2017). A combined EPR and MD simulation study of a nitroxyl spin label with restricted internal mobility sensitive to protein dynamics. J. Magn. Reson. *274*, 24–35. https://doi.org/10.1016/j.jmr.2016.11.001.
48. Lipari, G., and Szabo, A. (1982). Model-Free Approach to the Interpretation of Nuclear Magnetic Resonance Relaxation in Macromolecules. 1. Theory and Range of Validity. J. Am. Chem. Soc. *104*, 4546–4559. https://doi.org/10.1021/ja00381a009.
49. Freed, J.H. (1976). Theory of slow tumbling ESR spectra for nitroxides. In Spin Labeling Theory and Applications, L.J. Berliner, ed. (Academic Press), pp. 53–132.